Image and Vision Computing 160 (2025) 105574

Contents lists available at ScienceDirect

Image and Vision Computing

journal homepage: www.elsevier.com/locate/imavis

Deep learning-assisted 3D model for the detection and classification of knee arthritis

D. Preethi [a], V. Govindaraj [b], S. Dhanasekar [c], K. Martin Sagayam [d], Syed Immamul Ansarullah [e], Farhan Amin [f,*], Isabel de la Torre D'ıez [g,*], Carlos Osorio Garc'ıa [h], Alina Eugenia Pascual Barrera [h], Fehaid Salem Alshammari [i,j]

[a] Department of ECE, Vel Tech Rangarajan Dr. Sagunthala R&D Institute of Science and Technology, Chennai, India
[b] Department of ECE, Kalignar karunanidhi Institute of Technology, Coimbatore, India
[c] Department of ECE, Sri Eshwar College of Engineering, Coimbatore, India
[d] Department of ECE, Karunya Institute of Technology and Sciences, Coimbatore, India
[e] Department of Management Studies, University of Kashmir, North Campus, Delina, Baramulla 193103, Jammu & Kashmir, India
[f] School of Computer Science and Engineering, Yeungnam University, Gyeongsan 38541, Republic of Korea
[g] Department of Signal Theory and Communications, University of Valladolid, 23200 Valladolid, Spain
[h] Universidad Europea del Atl'antico, Isabel Torres 21, 39011 Santander, Spain
[i] Department of Mathematics and Statistics, College of Science, Imam Mohammad Ibn Saud Islamic University (IMSIU), Riyadh, Saudi Arabia
[j] King Salman Center for Disability Research, Riyadh 11614, Saudi Arabia

ARTICLE INFO

Keywords:
Deep learning
Disease classification
Knee osteoarthritis
Magnetic resonance imaging

ABSTRACT

Osteoarthritis (OA) affects nearly 240 million people worldwide. It is a common degenerative illness that typically affects the knee joint OA causes pain, and functional disability, especially in older adults is a common disease. One of the most common and challenging medical conditions to deal with in old-aged people is the occurrence of knee osteoarthritis (KOA). Manual diagnosis involves observing X-ray images of the knee area and classifying it into different five grades. This requires the physician's expertise, suitable experience, and a lot of time, and even after that, the diagnosis can be prone to errors. Therefore, researchers in the machine learning (ML) and deep learning (DL) domains have employed the capabilities of deep neural network (DNN) models to identify and classify medical images in an automated, faster, and more accurate manner. Combining multiple imaging modalities or utilizing three-dimensional reconstructions can enhance the accuracy and completeness of 2D Images in diagnostic information. Hence to overcome the drawbacks of 2D imaging, the reconstruction of 3D models using 2D images is the main theme of our research. In this paper, we propose a deep learning-based model for the detection and classification of the early diagnosis of arthritis. It is a four-step procedure starting with data collection followed by data conversion. In this step, our proposed model deforms the target's convex hull to produce a 3D model. Herein, a series of 2D photos is utilized, along with surface rendering methods, to create a 3D model. In the third step, the feature extraction is performed followed by mesh refinement. The chamfer loss is optimized based on the rotational shape of the leg bones, and subsequently, the weight of the loss function can be allocated to the target's geometric properties. We have used a modified Gray Level Co-occurrence Matrix (GLCM) for feature extraction. In the fourth step, the image classification is performed and the suggested optimization strategy raises the model's accuracy. A comparison of results with current 3D reconstruction techniques proves that the suggested method can consistently produce a waterproof model with a greater reconstruction accuracy. The deep-seated intricacies and distinct patterns across arthritic phases are estimated through the extraction of complicated statistical variables combined with power spectral density. The high-dimensional data is divided into separate, easily observable groups using the Lion Optimization Algorithm and proposed distance metric. The F1 Score and Jaccard Metric showed an average of 0.85 and 0.23, indicating effective differentiation across clusters.

* Corresponding authors.
E-mail address: farhanamin10@hotmail.com (F. Amin).

https://doi.org/10.1016/j.imavis.2025.105574
Received 4 December 2024; Received in revised form 8 April 2025; Accepted 28 April 2025
Available online 12 May 2025

1. Introduction

A common degenerative illness that typically affects the knee joint is osteoarthritis (OA), which causes pain and functional disability, especially in older adults is a common disease. The diagnostic and monitoring techniques for OA are crucial because it has significant global prevalence and detrimental effects on everyday activities. Conventional diagnostic modalities like Computed Tomography (CT) scans, Magnetic Resonance Imaging (MRI), and X-rays [1] are reliable but have several drawbacks, including high prices, radiation, and impracticability for routine monitoring, etc. Thus, a monitoring system that is dependable, affordable, and non-invasive is essential.

For instance, similar techniques are deployed in other medical conditions, e.g., cardiac-related problems, and are diagnosed using LV segmentation since it has a substantial impact on comprehending normal anatomy and the ability to discriminate between abnormal or diseased. The Mask R- Convolutional Neural Networks (CNN) model [20] performs better than SegNet architecture on evaluation metrics such as accuracy and precision. Hence, the neural architectures are deployed in this work.

To address the limitations of distributed data sharing, a novel federated ED framework based on the sequence perturbation privacy-preserving approach (FedED-SegNAS) is predominant in medical images. First, to address the lack of.

interpretability in deep learning models, fuzzy logic into CNNs could be incorporated to enhance their ability for expressing genetic ambiguity with high interpretability and tolerable accuracy. Employing the neural architecture search method to improve the federated neural architecture, especially using the particle swarm optimization technique to automatically search for the ideal neural architecture at various phases in Federated Learning (FL) to improve communication efficiency [19].

The standard methods for analyzing arthritis are X-ray and MRI [1]. X-ray is an imaging diagnostic tool used for arthritis. Arthritis is a group of conditions characterized by inflammation of the joints, leading to pain, swelling, stiffness, and reduced joint mobility. X-rays help diagnose and monitor arthritis by providing images of the bones and joints. As the cartilage in the joint wears away due to arthritis, the space between the bones may decrease. Osteophytes or bone spurs may develop around the edges of the joints. These are bony projections that can be seen on X-rays.

Different types of arthritis may have specific characteristics visible on X-rays. For example, in OA, X-rays show characteristic joint changes, such as osteophytes and joint space narrowing. In Rheumatoid Arthritis (RA), X-rays may reveal signs of inflammation, joint erosion, and changes in the soft tissues around the joints. This helps the healthcare providers ensure accurate placement of medications into the affected joint. X-ray imaging for arthritis diagnosis and management is part of a comprehensive approach that includes clinical evaluation, medical history, and sometimes additional imaging studies to understand the condition entirely.

If the structure of joints is not as good as that of straight bones, bone deterioration cannot be seen on radiography [2]. Fig. 1 illustrates an X-ray image of a joint affected by arthritis. The patient may be diagnosed with arthritis based on the radiographic imaging. Thus, it is clear that the X-ray test has a higher explicitness and a lower sensitivity. MRI is a powerful imaging technique widely used in medical diagnostics, including assessing arthritis.

One of the primary advantages of MRI is its ability to provide detailed images of soft tissues, including cartilage, ligaments, tendons, and the synovium (lining of the joint). MRI can reveal changes in bone structure, such as erosions or bone marrow abnormalities, which are common in inflammatory arthritis. Contrast-enhanced MRI may enhance the visibility of active inflammation and assess the extent of bone involvement.

The locations of the cartilage tissue injury are depicted in Figs. 2(a) and 2(b). However, a hefty dose of radiation is emitted during an MRI scan and has adverse effects. MRI continuous scanning is becoming more problematic and causes erosion, so it's preferable to switch to a different non-invasive technique. X-rays or traditional CT/MRI scans are 2D. These valuable tools are used in medical diagnostics and have drawbacks. For example, 2D images provide limited depth perception, making it challenging to assess the spatial relationships between structures in three dimensions accurately. This limitation may lead to difficulties in precisely understanding the extent of abnormalities, especially in complex anatomical regions.

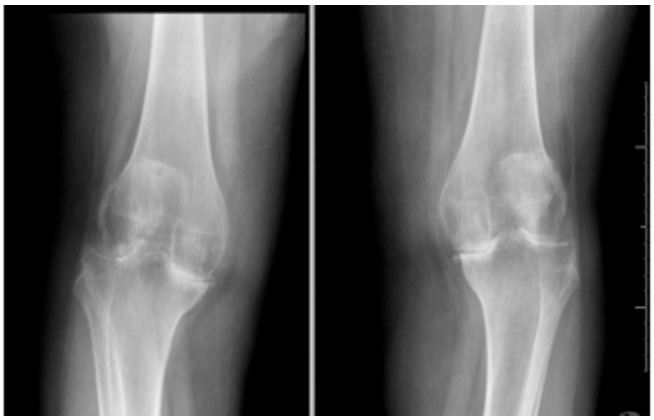

Fig. 1. Knee Osteoarthritis X-Ray.

In 2D imaging, overlapping structures can obscure the view of underlying or adjacent tissues. Superimposition in 2D imaging [3] may hinder accurately identifying specific structures, making it challenging to differentiate between different tissues or abnormalities. In addition, they have limited contrast for soft tissues. This limitation can make distinguishing between various soft tissues complex, potentially affecting the detection of subtle abnormalities or early stages of diseases. 2D images capture a static snapshot at a particular point in time. Dynamic changes, such as joint movements or blood flow, are poorly represented. This can limit the ability to assess functional aspects or the progression of certain conditions. 2D images may not provide detailed information about the texture and composition of tissues. Certain diseases manifest as changes in tissue texture, and these subtleties may be challenging to discern in 2D images alone. Recent advancements in medical imaging technologies aim to overcome some of these limitations. Techniques such as 3D imaging, multi-slice CT, and advanced MRI protocols provide more detailed spatial information and improve the overall diagnostic capabilities. Combining multiple imaging modalities or utilizing three-dimensional reconstructions can enhance the accuracy and completeness of diagnostic information. Hence, to overcome the drawbacks of 2D imaging, the reconstruction of 3D models using 2D images is the main theme of our research.

The motivation of this research is that traditional 2D imaging methods (e.g., X-rays) do not provide comprehensive details of knee joint structures. Thus, we should develop an advanced 3D imaging model for enhanced visualization. Herein, we propose a 3D model that offers a more precise visualization of the anatomical features, improving diagnostic accuracy for knee arthritis. It is a four-step procedure. In the first step, the data is collected. We have used public medical imaging data. In the second step, the data conversion is performed. In this step, our proposed model deforms the target's convex hull to produce a 3D model. Herein, a series of 2D photos is utilized, along with surface rendering methods, to create a 3D model. In the third step, the feature extraction is performed. In this phase, the mesh refinement, the chamfer loss, is optimized based on the leg bones' rotational shape; subsequently, the weight of the loss function can be allocated to the target's geometric properties. We have used a modified Gray Level Co-occurrence Matrix (GLCM) for feature extraction. In the fourth step, image classification is

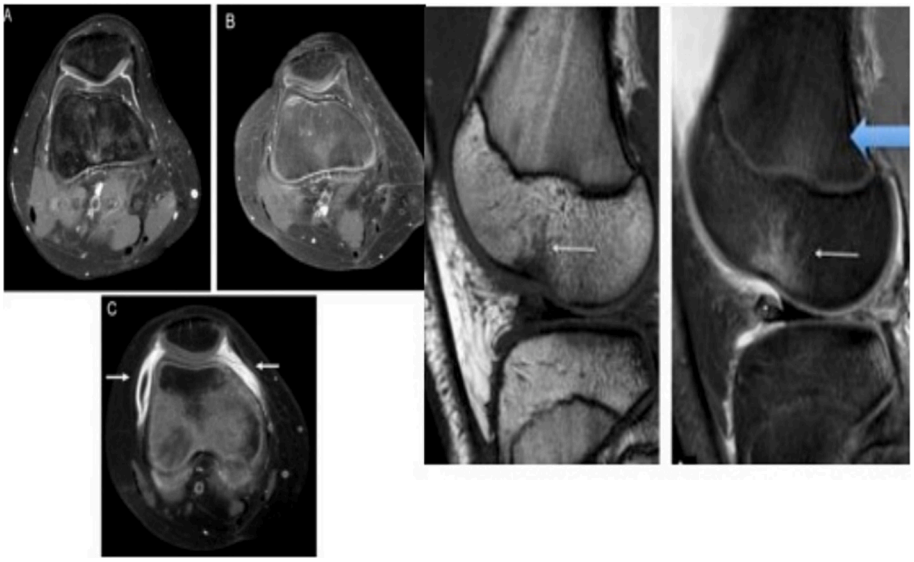

Fig. 2. (a) Top view of the knee joint using MRI scan; (b) Kinematic analysis of the knee joint with an MRI scan.

performed, and the suggested optimization strategy improves the model's accuracy. The key features of our proposed model are given below.

- Early Detection: Our proposed 3D model helps detect early signs of arthritis by offering detailed assessments of joint degeneration, which may not be apparent in standard 2D images.
- Tailored Interventions: By creating patient-specific 3D models, clinicians can assess the severity and progression of arthritis more accurately, leading to personalized treatment plans, whether physical therapy, medication, or surgical intervention.
- Surgical Precision: In cases requiring surgery, 3D models allow surgeons to plan and execute procedures more precisely, reducing the risk of complications and improving outcomes.
- Reduced Need for Invasive Tests: With more accurate 3D classifications, the need for more invasive diagnostic procedures like arthroscopy can be reduced.
- AI and Machine Learning Integration: Integrating machine learning and AI techniques with 3D modeling can automate the Classification of knee arthritis, improving the efficiency of diagnoses and reducing the workload on radiologists and clinicians.
- Faster Diagnosis: Automated classification systems using 3D models can provide quicker diagnostic results, essential for early treatment and better patient outcomes.
- Reduced Healthcare Costs: By improving the accuracy of early diagnosis and minimizing the need for more invasive procedures, 3D model-based Classification could potentially reduce long-term healthcare costs associated with managing knee arthritis.

Our key contributions are given below.

Our Contribution

- We propose a non-invasive approach used for the early detection and Classification of knee arthritis is explored through 3D image reconstruction derived from 2D images.
- In this research, complex nuances and unique patterns observed throughout different stages of arthritis are analyzed by extracting intricate statistical features combined with power spectral density.
- The proposed model received high-dimensional data is then segmented into distinct, easily interpretable groups using a modified Lion Optimization Algorithm and a novel distance metric.
- In our proposed model, the chamfer loss is minimized and optimized based on the rotational alignment of the leg bones, allowing the loss function to be weighted according to the target's geometric characteristics, using appropriate standard deviation values.
- We have performed the experimentation and the quantitative evaluation of the proposed models is evaluated using state of art deep learning models.

In the related work section, we discuss imaging and Classification. Furthermore, the feature extraction using the GLCM and the classification of arthritis using the Lion Optimization Algorithm (LOA) are discussed in section 3. Section 4 reviews and wraps up the simulation results.

2. Related work

Three-dimensional reconstruction technology based on CT images is mostly used in medicine to calculate the best site for radiation therapy and to simulate general surgical procedures. Many studies on the 3D reconstruction of medical pictures have been done recently. Some researchers employ traditional reconstruction algorithms like volume rendering and surface rendering to rebuild medical pictures. In [4], segment pulmonary nodules using Mask RNN and then apply the ray casting approach to reconstruct the target. In [5], 3D reconstruction of head CT data using the marching cubes and ray casting algorithms, respectively. Certain researchers have enhanced the reconstruction algorithm. In [6], based on visual hyper-spherical mapping, a technique to rebuild a watertight 2-manifold 3D bone surface model from CT scans is presented. This technique uses CT scans to create a 3D model of the femur and hip bones.

Nevertheless, the model failed to create a watertight surface at the right femur because of the impact of the CT slice's significant thickness. In [7] provide a sophisticated 3D reconstruction approach for ray casting that can minimize the number of rays by choosing the right bounding box. This approach can save memory and reconstruction time compared to the conventional methodology. There is a projection link between the point cloud and the triangular mesh. The sparse coefficient matrix is constructed using this relationship. The dictionary and matrix should then be updated iteratively using the objective function to complete the reconstruction. A few grouping techniques in the lettering define RA. MATLAB has refined several forms of support vector machines, such as polynomial-based Support Vector Machines (SVMs), Pearson-based SVMs, Gaussian-based SVMs, SVM with a straight section, Logistic Regression, Naïve Bayes, and Multi-Layer Perception (MLP). Strategic regression analysis returns class probabilities by taking an instantaneous

combination of vectors and applying a sigmoid limit to it. Usually, limits are established by assessing the most remarkable probability. A Bayesian classifier determines the likelihood of a class of given features by utilizing Bayes conjecture and a strong desire for self-sufficiency. As a result, the component factor allocations are self-sufficient and do not pose a financial burden on the class. The central 60 points of a multilayer perceptron, often called a neural network, are organized in several layers to create a network. Regressive proliferation of faults can lead to the oversight of the construction of frameworks. The information in a vector of information will be distributed using the yield evaluation methodology.

To maximize the edge between data classes, the SVM is a coordinated learning process that uses a large amount of data [8]. SVMs use input data that has been computed using the best edge hyperplanes as aiding vectors to present the perceptive metrics required for decision-making depending on fresh information. Consequently, SVMs offer parcel works that attempt to partition data that is difficult to separate inside their proprietary space into other component spaces better. Research on ensemble classifiers is distinct from different fields. The notion of a classifier was brought up by the fact that specific articles generate a range of mistakes, which motivates the results party to reduce differentials and produce more accurate results.

Using K-implies cluster analysis, an early diagnosis of rheumatoid infection is also attempted by considering four distinct criteria, specifically clinical information about the Rheumatoid Factor, SJC, anti-CCP, and ESR [9]. After K = 4 was chosen, the data from 60 patients was split up into four categories. The study's findings suggest that two of the four components may be able to predict rheumatoid joint inflammation, according to the K-implies grouping computation. This categorization model indicates that 84% of the assessment results are positive. Also, datasets that included randomly chosen data from 300 patients at Vanderbilt University Medical Centre were examined using electronic health records, Natural Language Processing (NLP) frameworks, and standardized information.

In [10] suggested utilizing segment data and clinical data gathered in the first two years after diagnosis to utilize Random Survival Forests (RSF) to forecast the onset of RA. Their study's findings indicate that the mean total error using testing and preparation data is 0.233 and 0.187, respectively. The time-dependent explicitness and affectability, using a time scale of 1 and 7 years, are, respectively, 0.79–0.80 and 0.43–0.48. Furthermore, the categorization of different infections based on groups and individuals has been discussed. [11] Recently shown that group methods may analyze valvular heart disease with three classifiers: Support Vector Machine (SVM), Multilayer Perceptron (MLP), and K-Nearest Neighbors (KNN). Lung runnet classification, filter design, and fault classification are discussed in [15–17].

[21] Deep Learning has revolutionized medical image processing by enabling automation in tasks like segmentation, classification, and reconstruction. U-Net remains a cornerstone architecture for image segmentation, particularly in biomedical applications. Recent advancements, such as Attention U-Net, improve feature extraction by focusing on relevant regions, enhancing segmentation accuracy [22].

Generative Adversarial Networks (GANs) have been employed in image reconstruction to synthesize high-quality images from noisy or incomplete data. Autoencoders have also been used for dimensionality reduction and reconstruction in volumetrics. Furthermore, CNNs and their derivatives, such as ResNet [23], have successfully classified disease severity from imaging datasets. However, challenges persist, including the scarcity of annotated datasets and the need for explainable AI in clinical applications [24]. Transfer learning and synthetic data augmentation techniques are frequently adopted to address these issues [25].

The discussions show that a non-invasive diagnosis for the computation of continuous data with accuracy is the key objective of the focus of the research. This could be achieved through effective image processing and classification techniques.

3. Proposed model

In this section, we present our proposed model. We have used a public dataset named Osteoarthritis Initiative (OAI). Limited data is collected by in-shoe sensing pads (By measuring the intensity of arthritis directly from patients).

3.1. Data collection

The Osteoarthritis Initiative (OAI) dataset is well-known in osteoarthritis research [18]. It is a longitudinal dataset that includes clinical, radiographic, and MRI data, making it valuable for studying the progression of knee osteoarthritis. The primary goal of the OAI is to understand the development and progression of knee osteoarthritis. The dataset includes a variety of data types, clinical data, radiographic images (X-rays), and magnetic resonance imaging (MRI) scans of the knee joint. This data is collected at multiple time points, allowing for examining changes in participants' conditions over time [19].

This longitudinal aspect is crucial for understanding disease progression. The results are also validated using the OAI Imorphics dataset for better accuracy and precision. The in-shoe system is another way to determine how foot pressure is distributed [12]. The four points that make up the sole support and bear most of the body's weight regarding balance. Its 15-ft pressure points cover all four 70-ft pressure points. Figs. 3 (a) & (b) show that the transducer was positioned beneath the hallux and the first, second, and fourth metatarsal heads. A test was conducted on over 50 persons across various age groups and genders, and it was concluded that about 90% of the individuals were accurately recognized.

The text file contains the dataset's collected data, which are then saved for later analysis. The value of a 16 × 16 matrix is further transformed into 256 87 single-line data and saved in a CSV (Comma-Separated Value) format. For the relevant patient, this CSV file and the target value are regarded as labeled data. Subsequently, the CSV file's 256 sensing point values are transformed into a heat map image for simple interpretation. The jet map algorithm is used to do this heat map conversion and determine the lowest and greatest pressure values in this algorithm, then scale the pressure values [16].

The scaling from minimum to maximum, each set of values is given a color that is identified using pressure. For instance, the intermediate values will be colored by the lowest and most significant values, which are represented by the colors blue and red, respectively. The output image is displayed in Fig. 4 using a jet map. We can see that most colors are smoother and more precise. These images are not clear. Therefore, we have used the Keiser approach to get smooth pictures. The refined images are cleared using machine learning algorithms to handle and produce better classification results.

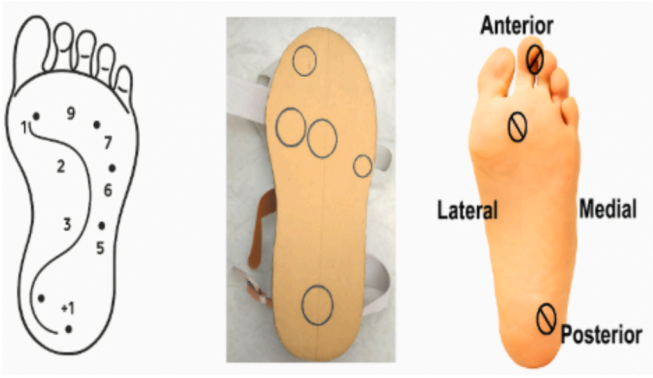

Fig. 3. (a) Pressure locations on the foot (b) The basis for biometric identification is variations in the foot pressure pattern.

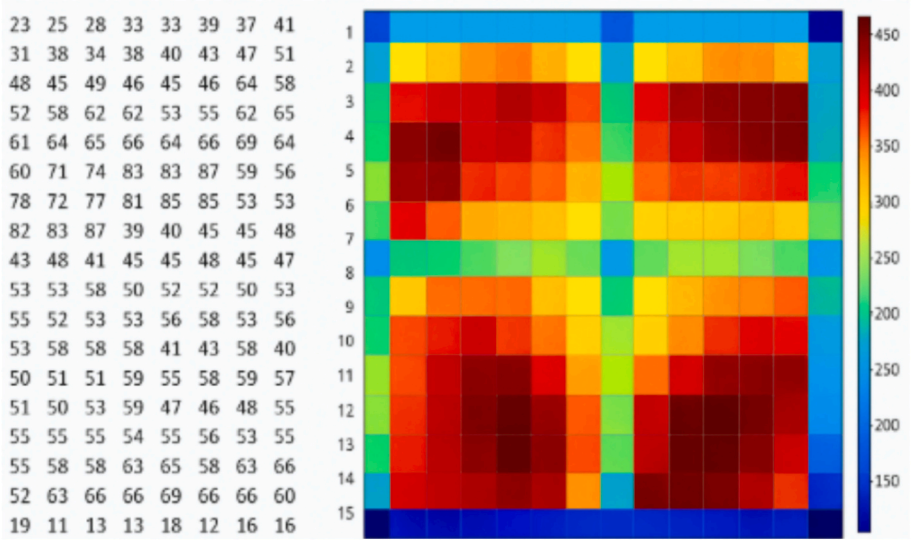

Fig. 4. (a) Data collected from Pressure locations on the foot (b) Heat Map analysis of a foot.

3.2. Data conversion

This section presents the conversion of 2D images to 3D meshes. This process involves creating a three-dimensional representation from two-dimensional data. A 2D image is chosen for conversion into a 3D mesh. Ideally, the image has distinguishable features and clear contrasts. We have used edge detection to highlight prominent features in the image. This helps identify boundaries between different regions. Consider each pixel in the image as a node in the mesh. The grayscale intensity of the pixel can be used as a basis for the mesh height.

The following steps are followed for the texture mapping of 3D images [12].

1. Height Map Generation: Convert the 2D image into a height map, where pixel values represent elevations. Darker regions may correspond to lower elevations, while lighter regions may represent higher elevations.
2. Extrusion: Extrude the 2D image along the height axis based on the values in the height map. This extrusion creates a three-dimensional effect.
3. Mesh Pooling: The pooling operation reduces the number of vertices and faces, effectively downsampling the mesh, as shown in Fig. 5 and See Fig. 6.)
4. Mesh Smoothing: Apply smoothing algorithms to refine the mesh and create a more visually appealing 3D representation.
5. Texture Extraction: Extract textures from the original 2D image.
6. Texture Mapping: Apply the extracted textures onto the corresponding regions of the 3D mesh. This step enhances the visual realism of the 3D representation.
7. Manual Refinement: Depending on the quality of the initial results, manual refinement of the mesh may be necessary to achieve the desired outcome.

Fig. 6. shows the reconstruction process starts with acquiring 2D images from medical imaging modalities like MRI, CT, or X-rays. Each image can be represented as a discrete intensity function: $I(x,y) : R2 \rightarrow R$ where $I(x,y)$ denotes the intensity value at pixel coordinates (x,y). The 3D volume is reconstructed by stacking these 2D slices along the z-axis to form a 3D grid of voxels: $V(x,y,z) : R3 \rightarrow R$ where $V(x,y,z)$ represents the intensity at voxel (x,y,z). Surface reconstruction involves extracting isosurfaces from the 3D voxel data using methods such as the marching cubes algorithm. An isosurface is defined as the set of points satisfying: $S = \{(x,y,z) | V(x,y,z) = T\}$ where T is a threshold intensity value. The

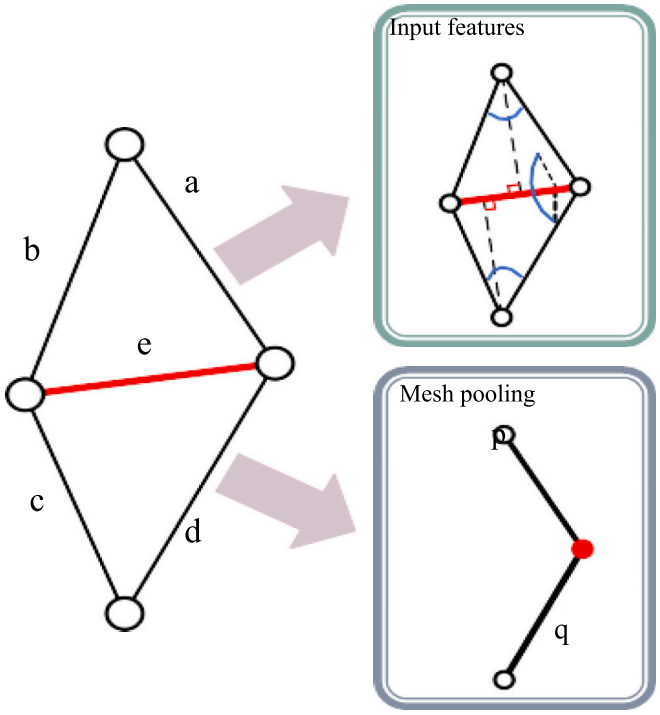

Fig. 5. Convolution of edge features (a-e) during Mesh Pooling.

algorithm computes triangular meshes to approximate S. For accurate reconstruction, slices are aligned using rigid or non-rigid transformations.

A transformation matrix T in (1) typically consists of rotation (R) and translation (t) components, where $R \in R^{3\times3}$ and $t \in R^3$.

$$T = [R\ t\ 0\ 1]..\tag{1}$$

3.3. Feature extraction

We have used the GLCM [13] for feature extraction. Before Classification, the image dataset is once more pre-processed using a neural network that has already been trained. The procedure of extracting features uses the GLCM. This approach characterizes the coarseness and smoothness of the pictures. It provides specific characteristics

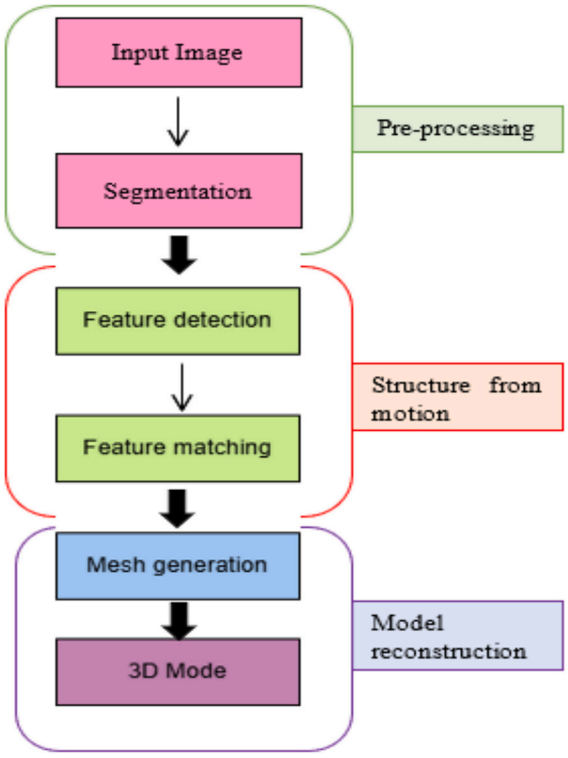

Fig. 6. Flow diagram depicting the 3D model of an input 2D image.

depending on the image dataset for categorization [10]. The dataset is classified using the chosen ten classifier methods such as k-Nearest Neighbor (k-NN), Naïve Bayes (NB), SVM, Particle Swarm Optimization (PSO), Ant Colony Optimization (ACO), Social Spider Algorithm (SSA), Cockroach Swarm Optimization (CSO), Lizard Learning Algorithm (LLA), African Wild Dog (AWD) and LOA is shown in Fig. 7.

Algorithm 1 is a matrix that represents the joint probability of two pixel intensities occurring together at a given spatial relationship. The GLCM is calculated by comparing each pixel with its neighboring pixels in a specified direction. The matrix elements (GLCM entries) correspond to the frequency of co-occurring intensity pairs [13].

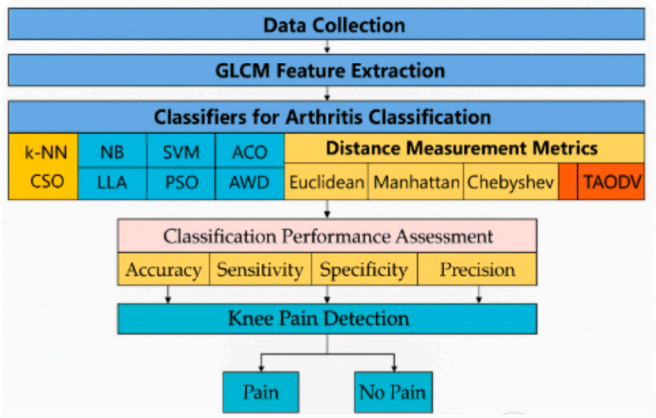

Fig. 7. Arthritis Data Classification.

Algorithm 1: Feature Extraction Algorithm

1. Read an image from the dataset
2. Convert the image to grayscale
3. Specify parameters
4. Calculate GLCM based on previous input
5. Extract features: Contrast, energy, homogeneity, correlation, entropy, and dissimilarity

We have suggested a modification in GLCM is a square matrix C of size G × G, where:

$$C(i,j) = \sum_{(p,q)}^{(p,q)} \begin{cases} 1, if\ I(p,q) = i\ and\ I(p+\Delta x, q+\Delta y) \\ = j, 0, otherwise..... \end{cases} \quad (2)$$

Where (p,q) is a pixel location in the image, Δxand Δy defines the relative position of the neighboring pixel (direction of comparison), and i and j are gray levels (ranging from 0 to G − 1).

Herein, we normalize and divide each element by the total number of co-occurring pixel pairs.

$$Cnorm(i,j) = \frac{C(i,j)}{\sum_{i=0}^{G-1}\sum_{j=0}^{G-1} C(i,j)} \ldots \quad (3)$$

Step 3 From the normalized GLCM, several statistical texture features are computed. Some common features include: Contrast = $\sum_{i=0}^{G-1}\sum_{j=0}^{G-1}(i-j)^2.Cnorm(i,j)$.

This measures the intensity contrast between a pixel and its neighbor over the entire image.

$$\text{Homogeneity} = \sum_{i=0}^{G-1}\sum_{j=0}^{G-1}\frac{Cnorm(i,j)}{1+|i-j|} \quad (4)$$

If the limit of agreement range is narrow, the two methods agree well, ensuring reliable RA severity grading i.e.,

Range = d ± 1.96sd where,

$$sd = \sqrt{\frac{1}{n-1}\sum_{i=1}^{n}(X1i - X2i - d)^2} \quad (5)$$

The GLCM for the image is computed in different directions, and the GLCM features such as contrast and homogeneity are extracted. These features are fed as input for a machine learning classifier to categorize images based on their texture.

3.4. Image classification

We have used a modified Lion Optimization Algorithm (LOA), a nature-inspired optimization algorithm based on the social behavior of lions. It was introduced as a metaheuristic optimization algorithm in 2016 [14]. The algorithm is designed to simulate the cooperative hunting behavior of lions in nature to find optimal solutions to optimization problems. Algorithm 2 shows the working mechanism.

Algorithm 2: LOA Algorithm

1: Generate random samples of lions as the initial population.
2: Initiate pride and nomad lions with %N and %S, respectively.
3: In each pride, some percentage of female lions go hunting and the rest will mate with resident lions for strong cubs. If a male lion is weak, it will send out of pride as a nomad
4: Male and female lions roam in the search space for nomads. If the nomads mate, strong cubs will come, or else prides might be attacked by nomads
5: some females with an immigration rate would roam as nomads.
6: if no termination condition is achieved, go to step 3.

The positions of lion at random for encircling the prey. The inspiration of this algorithm is by the fact that the opposition of the prey towards the attack of lion group is denoted by $\overset{\vee}{X}(\overset{\vee}{x_1}, \overset{\vee}{x_2}, \overset{\vee}{x_3}, \ldots \overset{\vee}{x_N})$ where $x_i \in [a_i, b_i]$is an optimum solution over a space limit of 'N' for a real coordinates 'a' and 'b'.

$$PREY = \sum Hunters(x_1, x_2, \ldots x_{NVar}) \Big/ No.ofHunters \tag{6}$$

For every new change in position of prey is given by,

$$PREY' = PREY + rand(0,1) \tag{7}$$

(3.36)

The change in position or alignment of hunters for encircling the prey is,

$$Hunter' = \begin{cases} rand(Hunter, PREY), Hunter < PREY \\ rand(Hunter, PREY), Hunter > PREY \end{cases} \tag{8}$$

The success rate at which an optimum solution is attained is defined by,

$$S(i,t,p) = \begin{cases} 1, \mathrm{Best}^{t}_{i,p}, p < Best_{i,p}^{t-1} \\ 0, Best_{i,p}^{t} = Best_{i,p}^{t-1} \end{cases} \tag{9}$$

3.4.1. Proposed TAODV as distance metric in classifier

Based on the idea deduced from wireless ad-hoc networks, a modification is suggested in the previously stated classifier in terms of distance measurement between two neighbors is presented to prevent misclassification. To make it easier to extract the type of arthritis and its extent, this metric is incorporated into classifiers to assess the trust of its neighbors with an established threshold which is shown in Table 1.

The values in its opinion about a neighboring node are used to modify predefined trust judgment rules. The weight representation wAB = (bAB, dAB, uAB) includes the opinion of belief, disbelief, or uncertainty.

- *bAB*: To prevent outliers, the belief of node A on node B will be computed based on the compactness of node B's five nearest neighbors. The degree of belief increases with decreasing distance.
- *dAB*: The distance equation $|A - B|$ is used to compute the disbelief from node *A* to node *B*. Disbelief increases as distance increases.
- *uAB*: The degree of uncertainty between nodes *A* and *B* is calculated using entropy. Less entropy means that there is less uncertainty between nodes A and B.

Table 1
Proposed Distance Metric for LOA Classifier.

Weight (wAB)	Decision	Grouping underclass
$wA\,B >$ Threshold	Belief	No Pain
$wAB <$ Threshold	Disbelief	Pain
$wA\,B =$ Threshold	Uncertainty	Compared against previous judgment: 1. no previous opinion weight is updated as (0, 0, 1) else 2. considered as noise if uncertainty is high

4. Experimentations, results, and discussion

There are four grades of arthritis whose statistical features are shown in Fig. 7. The boxplot for mean values showcases a narrow distribution for Grade 1 OA, suggesting a consistent disease manifestation at this preliminary stage. In contrast, the wider distribution observed for Grades 2, 3, and 4 signifies the varied manifestations of disease progression, arising from varying degrees of osteophyte formation, cartilage degradation, synovial inflammation, and alterations in joint space [4]. The distribution of median values, another measure of central tendency, exhibits a wider range in Grade 3 OA. This distribution variation, indicative of significant divergence in the middle values of the knee sound signals, is likely attributable to the moderate to severe osteophyte formation and joint space narrowing typical of this stage.

Fig. 8, Boxplot represents the statistical properties of four grades in the Arthritis dataset. The efficacy of the resulting cluster formation was critically evaluated by adopting two recognized metrics: *F*1 Score and Jaccard Metric. These quantifiers collectively provide a benchmark for assessing the aptness of the implemented clustering. A dual-phase approach was applied to compute the *F*1 score for each data point. The average intra-cluster distance, denoted as 'a', was initially calculated for each point concerning all other corresponding points in its cluster. Thereafter, the mean nearest-cluster distance, represented as 'b', was computed, which reflects the average spatial distance between the point under consideration and all points about the closest cluster, excluding its own. The F1 score was then obtained by employing the formula: $F1\ Score = (b-a)/max(a,b)$ [27, 28].

This score essentially offers a normalized measure of the distinction between the intra-cluster and the nearest-cluster distances. The coefficient's range is from −1 to 1, with 1 implying a perfect match with its cluster, and − 1 suggesting a better fit with a different cluster. Additionally, the Jaccard Metric was employed to assess the resulting cluster. A lower Jaccard Metric value indicates a superior clustering model, implying a more substantial separation among the clusters. This index measures each cluster's mean "similarity" with its most analogous cluster. Here, similarity is defined as the ratio of within-cluster distances to between-cluster distances as shown in Table 2. Comparative tests demonstrate that relative to existing 3D reconstruction techniques, the proposed method consistently generates a waterproof model with superior reconstruction accuracy, as shown in Fig. 9.

In the LOA classifier, the population size is chosen to be 20, and the tuning parameters are assumed to be 0.5 and 0.75, respectively, as shown in Table 3. The constant rand is maintained at 0.5. The range of the flock is set between the range (−25, 25) with a step size of 0.01. The PREY is decided upon the total number of attributes; hence is fixed at 6.0. The Hunt ratio is 0.1. Chamfer Loss and Cosine Similarity are essential in rheumatoid arthritis (RA) image analysis, enhancing accuracy in detecting joint deformities, bone erosion, and inflammation. Chamfer Loss helps compare predicted and actual joint structures, improving segmentation and tracking.

Disease progression in X-rays and MRIs. Cosine Similarity ensures precise feature matching, aiding in distinguishing RA-affected joints from healthy ones and monitoring changes over time. Integrating these techniques into deep learning models enhances automated RA diagnosis, enabling early detection and better treatment planning [26,27].

Table 3. shows the comparison in performance Metrics of ten classifiers. The performance of LOA is compared against various other classifiers such as k-nearest Neighbor (k-NN), Naïve Bayes (NB), Support Vector Machine (SVM), Particle Swarm Optimization (PSO), Ant Colony Optimization (ACO), Social Spider Algorithm (SSA), Cockroach Swarm

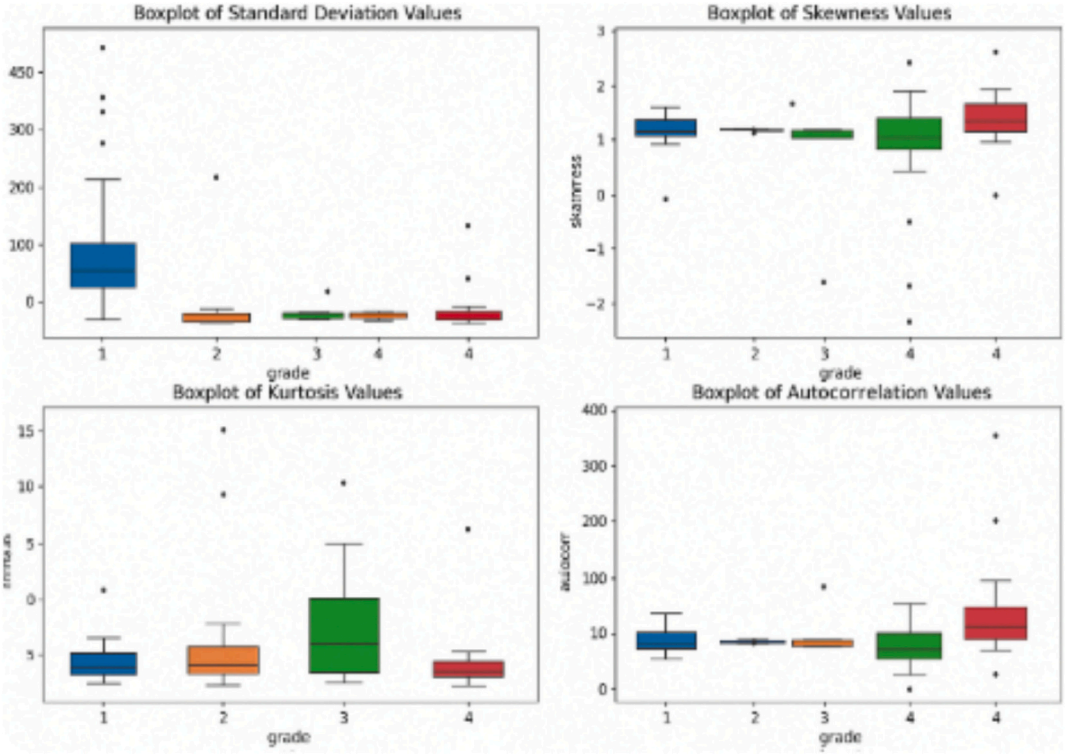

Fig. 8. Boxplot representing statistical properties of four different grades in the Arthritis dataset.

Table 2
The reconstruction accuracy of different weight distributions.

σ	chamfer loss	cosine similarity
1.75	0.082	0.19
1.5	0.07	0.22
1.25	0.075	0.47
1	0.057	0.54
0.5	0.012	0.63
0.25	0.010	0.78
0.15	0.36	0.48

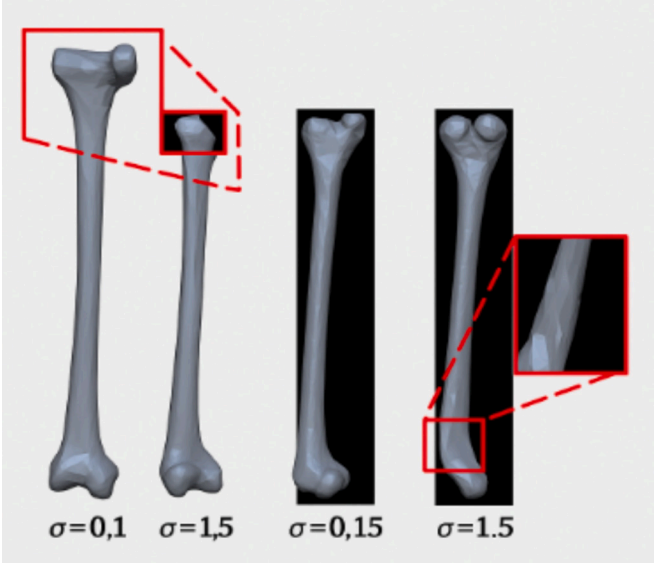

Fig. 9. 3D reconstructed Image of Bone.

Optimization (CSO), Lizard Learning Algorithm (LLA) and African Wild Dog (AWD). The efficient utilization of energy subsiding in nodes through a lifetime of static and mobile nodes for tracing the optimum solution under a search space is the major reason for the better performance of LOA. To achieve faster response and high sensitivity, static nodes are to be placed at the center of focus to all other neighbor nodes. Whereas the mobile nodes are supposed to be well distributed, to reduce execution time in response to quick chain processes but tend to increase power and consume more energy. Henceforth the difference in static and mobile nodes must be minimal for an energy efficient system. This in turn also ensures that there is devoid of traffic congestion for both the sample of collected data records.

5. Conclusion

Herein, we propose a non-invasive model for the early diagnosis and grading of knee arthritis using 3D Image reconstruction from 2D Images. The chamfer loss is reduced and is optimized based on the rotational shape of the leg bones. Subsequently, the weight of the loss function can be allocated to the target's geometric properties using suitable standard deviation values. The outcomes of the Gray Level Co-occurrence Matrix (GLCM) for feature extraction were followed by the modified Lion Optimization Algorithm (LOA) classification. Thus, the optimization strategy raises the model's accuracy to 90% due to a proposed distance metric named TAODV. We have performed several experiments, and the comparative tests show that, compared to current 3D reconstruction techniques, the suggested method can consistently produce a waterproof model with a greater reconstruction accuracy. It has 90% less chamfer loss and 30% more cosine similarity observed during reconstruction through effective transformation and analysis of 3D images. It is identified through the generalization experiment that this method also has good reconstruction accuracy for other bones. The deep-seated intricacies and distinct patterns across arthritic phases are estimated through the extraction of complicated statistical variables combined with power spectral density. The high-dimensional data is divided into separate, easily observable groups using the Lion Optimization

Table 3
Comparison of ten classifiers.

Classifier	Performance Metrics									
	Acc.	Er.R.	Sens.	Spec.	FPR	Prec.	F1	MCC	JM	BCR
k-NN	61.3	38.8	60.0	62.5	37.5	61.5	0.60	22.5	0.43	61.3
NBC	72.5	27.5	72.5	72.5	27.5	72.5	0.72	45.0	0.56	72.5
SVM	78.3	21.3	77.5	80.0	20.0	79.5	0.78	57.5	0.64	78.8
ACO	85.0	15.0	85.0	85.0	15.0	85.0	0.81	70.0	0.73	85.0
SSA	77.5	22.5	77.5	77.5	22.5	77.5	0.77	55.0	0.63	77.5
CSO	80.0	20.0	80.0	80.0	20.0	80.0	0.80	60.0	0.66	80.0
LLA	88.8	11.3	90.0	87.5	12.5	87.8	0.83	77.5	0.38	88.8
PSO	83.8	16.3	87.5	80.0	20.0	81.4	0.84	67.7	0.72	83.8
AWD	87.5	12.5	87.5	87.5	12.5	87.5	0.83	75.0	0.57	87.5
LOA	90.0	10.0	87.5	92.5	7.5	92.1	0.85	80.1	0.23	90.0

Algorithm and proposed distance metric. The F1 Score and Jaccard Metric showed an average of 0.85 and 0.23, indicating effective differentiation across clusters. Both Chamfer loss and cosine similarity play crucial roles in automated RA diagnosis. Chamfer Loss refines joint structure predictions, while Cosine Similarity improves RA feature comparisons. Integrating these methods has improved limit of agreement is between 0.082 and 0.36 respectively ensuring early detection, severity assessment, and personalized treatment planning for RA patients. The future direction of work focuses on simulating stress, strain, and load-bearing properties to assess functionality. In addition, modeling movement and interaction of bones and joints under physiological conditions shall also be considered.

CRediT authorship contribution statement

D. Preethi: Investigation, Conceptualization. **V. Govindaraj:** Methodology, Investigation. **S. Dhanasekar:** Resources, Methodology. **K. Martin Sagayam:** Validation, Supervision, Software. **Syed Immamul Ansarullah:** Methodology, Investigation. **Farhan Amin:** Resources, Project administration, Methodology, Data curation, Conceptualization. **Isabel de la Torre D'ıez:** Investigation, Funding acquisition, Formal analysis. **Carlos Osorio Garc'ıa:** Formal analysis, Data curation, Conceptualization. **Alina Eugenia Pascual Barrera:** Project administration, Methodology, Funding acquisition. **Fehaid Salem Alshammari:** Conceptualization, Formal analysis, Funding acquisition, Project administration, Writing – review & editing, Writing – original draft.

Funding

The authors extend their appreciation to the King Salman center For Disability Research for funding this work through Research Group no KSRG-2024-408.

Declaration of competing interest

The authors declare that they have no known competing financial interests or personal relationships that could have appeared to influence the work reported in this paper.

Acknowledgment

The authors extend their appreciation to the King Salman center For Disability Research for funding this work through Research Group no KSRG-2024-408.

Data availability

All relevant data are included in the manuscript.

References

[1] M.L. Chu, I.A. Gradisar, M.R. Railey, G.F. Bowling, Detection of knee joint diseases using acoustical pattern recognition technique, J. Biomech. 9 (1976) 111–114.
[2] C. Ma, et al., Knee joint pathology screening using time-domain multidimensional fusion feature and random forest, in: Proc. China Automation Congress (CAC), Xiamen, China, 2022, pp. 2194–2199.
[3] S. Nalband, A. Prince, A. Agrawal, Entropy-based feature extraction and classification of vibroarthographic signal using complete ensemble empirical mode decomposition with adaptive noise, IET Sci. Meas. Technol. 12 (4) (2018) 525–532.
[4] K. Umapathy, S. Krishnan, Modified local discriminant bases algorithm and its application analysis of human knee joint vibration signals, IEEE Trans. Biomed. Eng. 53 (3) (2006) 517–523.
[5] K.P.H. Pritzker, S. Gay, S.A. Jimenez, K. Ostergaard, J.-P. Pelletier, P.A. Revell, D. Salter, W.B. van den Berg, Osteoarthritis cartilage histopathology: grading and staging, Osteoarthr. Cartil. 14 (2006) 13–29.
[6] W. Fang, D. Lin, W. Kou, et al., Advances in medical image three-dimensional reconstruction system, Chin. J. Med. Phys. 39 (7) (2022) 823–827.
[7] W. Chao, R. Xuejiang, Application research of 3D reconstruction of auxiliary medical image based on computer, in: Big Data Analytics for Cyber-Physical System in Smart City BDCPS 2020 Advances in Intelligent Systems and Computing (AISC 1303) 2, 2021, pp. 106–112.
[8] T.R. Yuan, H.S. Zhang, H. Liu, et al., Watertight 2-manifold 3D bone surface model reconstruction from CT images based on visual hyper-spherical mapping, Math. Biosci. Eng. 18 (2) (2021) 1280–1313.
[9] S.S. Joseph, A. Dennisan, Three dimensional reconstruction models for medical modalities: a comprehensive investigation and analysis, Curr. Med. Imaging 16 (6) (2020) 653–668.
[10] L. Mescheder, M. Oechsle, M. Niemeyer, et al., Occupancy networks: Learning 3D reconstruction in function space, in: Proceedings of the 32nd IEEE/CVF Conference on Computer Vision and Pattern Recognition (CVPR), Long Beach, CA, 2019.
[11] M. Dorigo, L.M. Gambardellam, Ant colony system: a cooperative learning approach to the traveling salesman problem, IEEE Trans. Evol. Comput. 1 (2015) 53–56.
[12] K. Weinberger, J. Blitzer, L. Saul, Distance metric learning for large margin nearest neighbor classification, in: Proceedings NIPS, MIT Press, Cambridge, MA, 2006, pp. 1475–1482.
[13] Weijie Chen, Charles E. Metz, Maryellen L. Giger, Karen Drukker, A novel hybrid linear/nonlinear classifier for two-class classification: theory, algorithm, and applications, IEEE Trans. Med. Imaging 29 (2) (2006) 428–441.
[14] Wu Shinq-Jen, Wu Cheng-Tao, Computational optimization for S-type biology systems: cockroach genetic algorithm, Math. Biosci. (2013) 299–313, https://doi.org/10.1016/j.mbs.2013.07.019.
[15] Maziar Yazdani, Fariborz Jolai, Lion optimization algorithm (LOA): a nature-inspired metaheuristic algorithm, J. Comput. Des. Eng. (2025), https://doi.org/10.1016/j.jcde.2015.06.003.
[16] L.J. Ahmed, P. Malin Bruntha, S. Dhanasekar, V. Govindaraj, T.S. Krishnapriya, A. Ramjan Begam, An efficient heart-disease prediction system using machine learning and deep learning techniques, in: 2023 9th International Conference on Advanced Computing and Communication Systems (ICACCS), Coimbatore, India, 2023, pp. 1980–1985.
[17] V. Govindaraj, E. Chenguttuvan, D. Subramaniyam, Design of power and area efficient carry skip adder and FIR filter implementation, ECJSE 10 (1) (2023) 81–89, https://doi.org/10.31202/ecjse.1162711.
[18] J. Ramesh, S. Nithyadevi, V. Govindaraj, Fault classification in digital to analog converter using machine learning, Int. J. Electron. 1–20 (2024), https://doi.org/10.1080/00207217.2024.2429149.
[19] Abdul Sami Mohammed, Ahmed Hasanaath, Ghazanfar Latif, Abul Bashar, Knee osteoarthritis detection and severity classification using residual neural networks on preprocessed X-ray images, Diagnostics 13 (2023) 1380, https://doi.org/10.3390/diagnostics13081380.
[20] V. Govindaraj, S. Dhanasekar, K. Martinsagayam, D. Pandey, B.K. Pandey, V. K. Nassa, Low-power test pattern generator using modified LFSR, Aerosp. Syst. 7 (1) (2023) 67–74, https://doi.org/10.1007/s42401-022-00191-5.
[21] X. Wu, Y.-T. Zhang, K.-W. Lai, M.-Z. Yang, G.-L. Yang, H.-H. Wang, A novel centralized federated deep fuzzy neural network with multi-objectives neural

architecture search for epistatic detection, IEEE Trans. Fuzzy Syst. 33 (1) (2025) 94–107, https://doi.org/10.1109/TFUZZ.2024.3369944.

[22] M.A. Shoaib, K.W. Lai, J.H. Chuah, Y.C. Hum, R. Ali, S. Dhanalakshmi, H. Wang, X. Wu, Comparative studies of deep learning segmentation models for left ventricle segmentation, Front. Public Health 10 (2022 Aug 25) 981019, https://doi.org/10.3389/fpubh.2022.981019. PMID: 36091529; PMCID: PMC9453312.

[23] O. Ronneberger, P. Fischer, T. Brox, U-Net: Convolutional networks for biomedical image segmentation, in: International Conference on Medical Image Computing and Computer-Assisted Intervention (MICCAI), 2015, pp. 234–241.

[24] O. Oktay, J. Schlemper, L.L. Folgoc, M. Lee, M. Heinrich, K. Misawa, K. Mori, S. McDonagh, N.Y. Hammerla, B. Kainz, B. Glocker, D. Rueckert, Attention U-Net: Learning where to look for the pancreas, 2018 arXiv preprint arXiv:1804.03999.

[25] K. He, X. Zhang, S. Ren, J. Sun, Deep residual learning for image recognition, in: Proceedings of the IEEE Conference on Computer Vision and Pattern Recognition (CVPR), 2016, pp. 770–778.

[26] J. Thorston, A support vector method for multivariate performance measures, in: ICML '05: Proceedings of the 22nd International Conference on Machine Learning, 2005.

[27] A.A. Citarella, F. De Marco, L. Di Biasi, M. Risi, G. Tortora, Gene ontology terms visualization with dynamic distance-graph and similarity measures, in: Proceedings of the 27th International DMS Conference on Visualization and Visual Languages (DMSVIVA 2021), 2021.